Study of coupling and edge effects during ICRF heating experiments using an electrostatic antenna on textor

ARTICLE *in* FUSION ENGINEERING AND DESIGN · JANUARY 1989

Impact Factor: 1.15 · DOI: 10.1016/0920-3796(90)90059-F

11 AUTHORS, INCLUDING:

Raymond Koch
Forschungszentrum Jülich
198 PUBLICATIONS **1,082** CITATIONS
SEE PROFILE

B. Schweer
Forschungszentrum Jülich
268 PUBLICATIONS **3,065** CITATIONS
SEE PROFILE

Fusion Engineering and Design 12 (1990) 15–23
North-Holland

STUDY OF COUPLING AND EDGE EFFECTS DURING ICRF HEATING EXPERIMENTS USING AN ELECTROSTATIC ANTENNA ON TEXTOR

R. KOCH, P. DESCAMPS, F. DURODIE, X.M. SHEN *, G. VAN OOST and R. VAN NIEUWENHOVE

Laboratoire de Physique des Plasmas – Laboratorium voor Plasmafysica, Association "Euratom–Etat Belge" – Associatie "Euratom–Belgische Staat", Ecole Royale Militaire – Koninklijke Militaire School, B-1040 Brussels, Belgium

B. SCHWEER and Y.T. LIE

Institut für Plasmaphysik des Forschungszentrum Jülich GmbH, Association "Euratom-KFA", D-5170 Jülich, Fed. Rep. Germany

K. MATSUMOTO

Dept. of Electrical Eng., Faculty of Engineering, Yamagata University, Yonezawa, 992 Japan

R.A. MOYER

Institute of Plasma and Fusion Research, University of California, Los Angeles, CA 90024, USA

S. SHINOHARA

Dept. of Physics, Faculty of Science, University of Tokyo, Bunkyo-ku, Tokyo 113, Japan

An electrostatic type of antenna has been tried on TEXTOR allowing a maximum of 340 kW to be coupled to the plasma during long pulses (0.5 s). Possibly due to mechanical problems, the voltage stand-off was found to be only half that of the regular fast wave antenna. The coupling capability itself, in terms of power coupled for a given maximum voltage on the antenna, is also a factor of two lower than that of the fast wave antenna. The coupling resistance does not show the (theoretically expected) characteristics of an ion Bernstein wave coupler; first theoretical investigations indicate that this antenna is mainly a fast wave launcher. The edge perturbations caused by this antenna are almost negligible while bulk density increase is observed, leading to the conclusion that the particle confinement time improves during the RF pulse.

1. Introduction

During the first months of 1989, an electrostatic type of antenna (hereafter denoted ES) has been used on TEXTOR to try to couple high power in the ion cyclotron range of frequencies. This electrostatic launcher was obtained from a regular Fast-Wave (FW) antenna [1] by removing the electrostatic screen and replacing the short-circuit by an insulator. The so obtained launcher is made up of two adjacent boxes, with one current strap in each, and the two straps can be fed either in or out of phase. The primary aims of using such a launcher were: (a) as far as ion Bernstein waves could be launched, to investigate heating by this method; (b) to test the quality of electrostatic coupling from the point of view of resistance, edge effects and impurity production; (c) to investigate the consequences of operating an antenna without screen.

In the first part of this paper, the coupling properties and voltage stand-off performance of these antennas are described. In the second part, the effects of this type of power launching on the plasma edge are examined. Bulk plasma properties like heating, confinement etc, will not be adressed but will be the subject of future work. As,

* A.S. Hefei, P.R. China.

however, edge perturbations have to be judged in the light of what happens in the center, we briefly summarize here the findings of this study. Ion heating has been observed, generally with much lower efficiency than with the FW antennas [2,3], but sometimes with similar efficiency. The electron temperature decreases so as to maintain the same relation between T_e and n_e as in ohmic during the density rise caused by the RF. Radiated power and impurity increases are moderate but the loop voltage systematically increases during the RF. In all cases the electrostatic antenna could be operated without disruption.

2. Antenna system

The launcher is a modification of the system described in refs. [1,4] and consists of a pair of antennas, each composed of a central conductor enclosed in a box and protected by side limiters as shown in fig. 1. With respect to the system decribed in ref. [1], the screen has been removed, the short-circuit replaced by two ceramic insulators and the bottom of the antenna box has been covered with tiles to protect it against beam shinethrough. The two antennas of the pair were originally identical. However, during operation, the right (seen from the TEXTOR inside as in fig. 1) antenna box came down, due to unknown (mechanical) reasons, by 1 cm at the feedpoint and $\simeq 1.5$ cm at the upper tip. In addition, on the same right antenna, both ceramic supports broke and the central conductor itself came down inside the box. This central conductor has been damaged at spots toroidally aligned with the spacings between the side protection tiles, on the ion drift side only. This indicates the presence of a plasma flow to the central conductor along field lines at these locations. On the left antenna, one of the ceramic supports was broken and the other one was in the process of breaking but the whole left hand side antenna had remained in place. This damage can be considered as essentially unrelated to the ES type of operation of the antenna. Both central conductor surfaces showed some roughness caused by exposure to the plasma.

The date at which the lowering of the box and the breaking of the ceramic supports took place is unknown. These changes were observed *after* the operation, at the time the antenna was inspected. However, due to the lack of any discontinuity in the operation characteristics and properties of the antenna over the whole experimental period, we suspect that these events occurred early, i.e. before the first high power operation of the antenna.

This situation has several important consequences with regard to the interpretation of the results. First, in its lowered position the right antenna box nearly played the role of a poloidal limiter (its radius was 46.5 cm as compared to the normal ALT-II [5] limiter radius of 46 cm). Second, the direct toroidal plasma flow could significantly lower the antenna's voltage standoff. Third, as the generator power is split passively via a T, power unbalance between the two antennas may have taken place. This implies that maybe neither pure π nor pure 0 phasing could be imposed. Due to the unsensitivity of the line voltage waveform to asymmetry, the method [6]

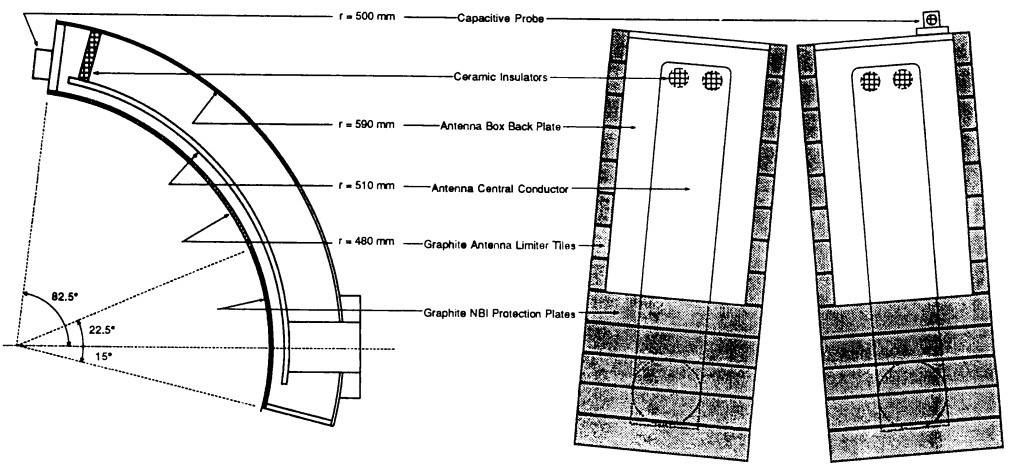

Fig. 1. Electrostatic launcher: poloidal cut (left) and view from the TEXTOR inside (right). The launcher is composed of two antennas, each one enclosed in a box. The location of the capacitive probe is also shown.

used to determine the antenna input impedance is unable to determine the unbalance ratio reasonably accurately. The values of the series resistance R_s and the phase ζ at the antenna input given in the following are therefore computed from the line voltage and power data assuming symmetry.

Only a very limited amount of time was devoted to the study of this antenna. Therefore, it is important to underline that the following results correspond to non-optimized operation. However, probably due to the problems described above, no clear experimental indication was found that operation could indeed be optimized.

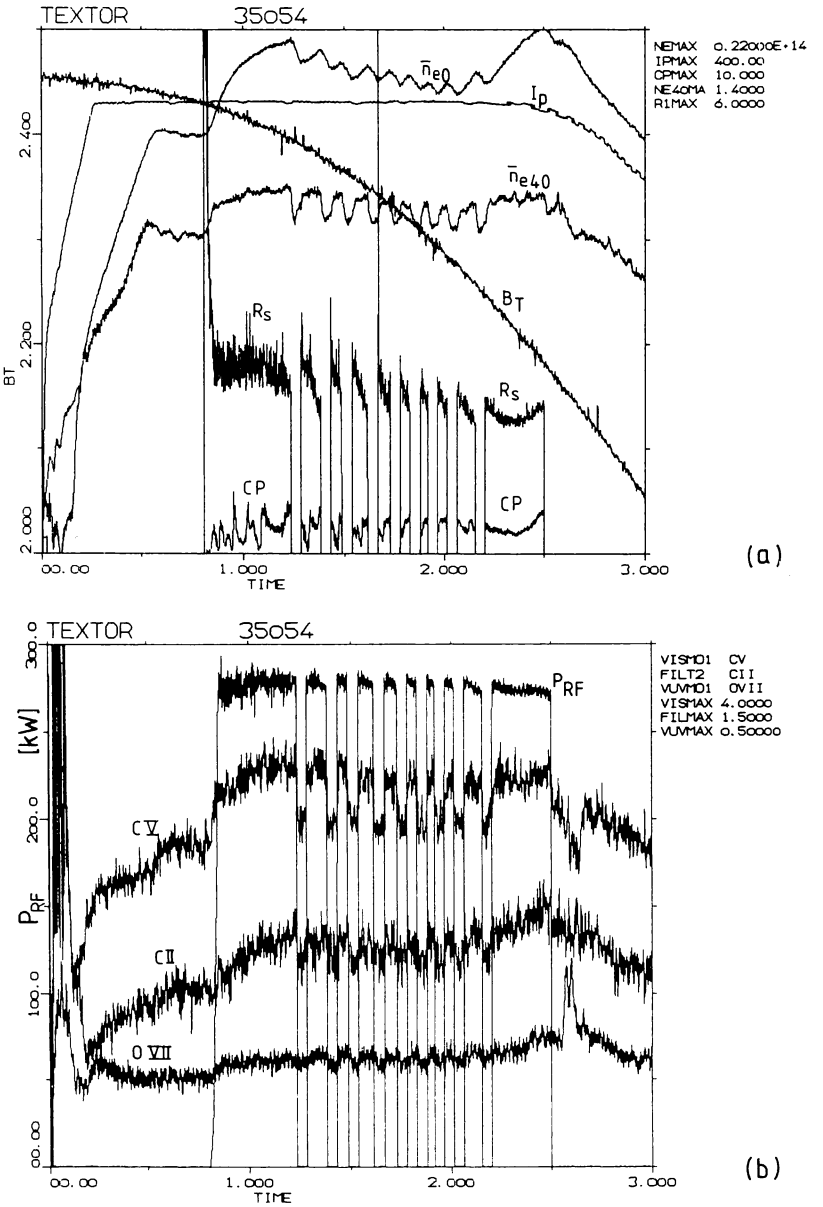

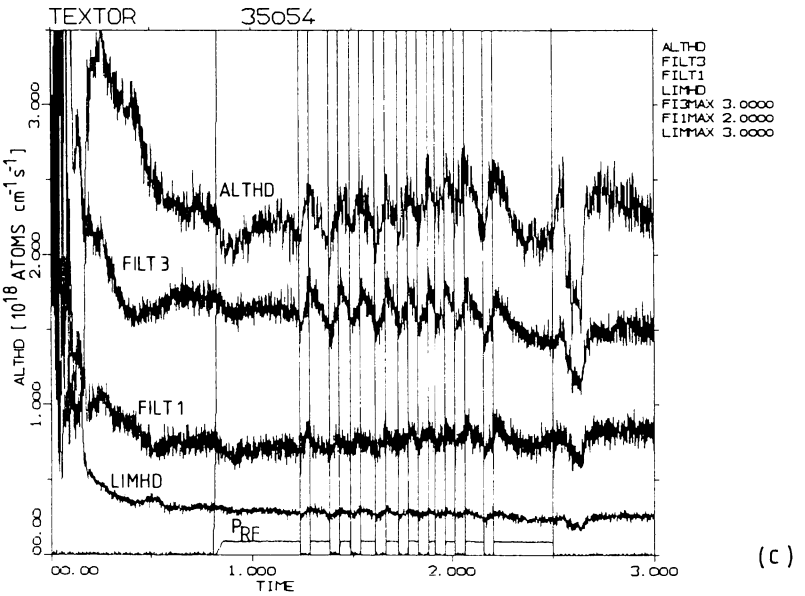

Fig. 2. TEXTOR shot 35054 with B_T scan. (a) Main parameters: toroidal magnetic field value at the plasma center B_T; central line-averaged density $\bar{n}_{e0}$; line-averaged density at $r = 40$ cm $\bar{n}_{e40}$; plasma current I_p; antenna series resistance R_s; capacitive probe signal CP. The B_T vertical scale is given explicitly; the other scales are $\bar{n}_{e0} \in [0, 2.2\times10^{19}\ \mathrm{m}^{-3}]$, $\bar{n}_{e40} \in [0, 1.4]$, $I_p \in [0, 400\ \mathrm{kA}]$, $R_s \in [0, 6\ \Omega]$, $CP \in [0, 10]$. The $\bar{n}_{e40}$ and CP scales are relative. (b) Power coupled to the plasma and impurity lines (signals are averaged over 5 ms). Except for P_{RF}, vertical scales are relative. (c) H_α/D_α signals at various locations at the edge. ALTHD is the flux at an ALT-II limiter blade located approximately 180° toroidally away from the ES antenna. FILT3 and FILT1 are the fluxes at the inboard bumper limiter measured respectively close to and 180° away from the ES antenna. LIMHD is the flux at a retracted ($r \lesssim 50$ cm) upper poloidal limiter located some 70° ($\simeq 2$ m) away from the antenna. Except for ALTHD for which the scale is given on the figure, scales are relative. P_{RF} is given for reference.

3. Experimental conditions

Fig. 2 summarizes a typical shot in nearly pure deuterium with a B_T scan. The RF is coupled using the ES antenna. Fig. 2a shows some important bulk plasma parameters, the antenna's series resistance and the capacitive probe signal. More details about this last measurement are given in a companion paper [7]. In fig. 2b, the brilliance of three impurity lines (characterizing the plasma bulk) is shown together with the time evolution of the RF power coupled to the plasma. Fig. 2c describes the D fluxes at the edge. The frequency is always $f = 29$ MHz. In shots with fixed B_T, the normal central toroidal magnetic field value is $B_T = 2.4$ T. This corresponds (theoretically) to an optimal launching for the IBW in pure D, with the 2nd harmonic close to the outboard antenna location and a nonlinear half harmonic damping layer $f = 1.5 f_{cD}$ located 10 cm inboard with respect to the plasma center. This experimental situation will hereafter be referred to as *standard shots*. Some shots were made in D–(H) at $B_T = 2$ T which is the normal condition for FW heating and will be referred to as FW *shots*. The plasma-current is 340 kA unless otherwise stated.

4. Coupling

4.1. Voltage standoff

The trace of the power coupled to the plasma P_{RF} on fig. 2b illustrates well a typical difficulty encountered when operating the ES antenna: the generator is periodically switched off because a breakdown is detected and can be restarted only after a certain time (although trying to restart at a few ms intervals). This looks more or less like if a maximum *energy* could be coupled without breakdown. However, the voltage standoff statistics of fig. 3 show that this is not the case in a multishot framework. Instead, this figure seems to indicate a voltage limitation near 12 kV at the antenna input, more or less independent of pulse length. Note

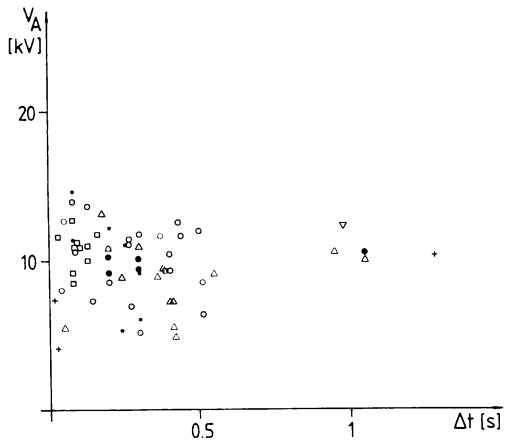

Fig. 3. Input antenna voltage V_A versus pulse length (without breakdown) for a large number of ES antenna pulses.

that the pulse length taken into account in this statistics is the longest one without breakdown in each shot, e.g. 0.35 s for the shot of fig. 2. The scarcity of long pulses at high voltage in fig. 3 does not only reflect a difficulty in reaching these conditions, but also the fact that we have not always tried to make the longest possible pulse. In this data no indication of dependence with respect to density has been found.

In terms of power, the maximum performance was $P_{RF} = 340$ kW (corresponding to a transmitted power $P = 400$ kW) during 0.5 s. The absolute maximum power was $P = 700$ kW but only for 10 ms.

The maximum voltage $V_A = 12$ kV at the antenna input corresponds to a maximum voltage on the antenna (in fact at the antenna tip) of $V_{Am} \simeq 17$ kV, which is nearly a factor of two lower than on the FW antenna.

4.2. Resistance

Each antenna shown in fig. 1 is composed of two parts, the first one covered with carbon tiles and the second facing the plasma. Note that the length of the radiating part ($l_1 = 0.473$ m) is significantly shorter than the radiating part of the original FW antenna (the length of the covered part is $l_2 = 0.237$ m). The vacuum (i.e. without plasma) electrical characteristics of both antenna parts have been determined by fitting over a wide range of frequencies (10–110 MHz) the experimental antenna input impedance to transmission line formulae. In the presence of plasma, we assume that the covered part of the antenna is unchanged. For the radiating part, we assume that the specific resistance R_2 and inductance L_2 keep the same value as in vacuum while the capacitance is changed by the plasma and radiation to the plasma is represented by a nonvanishing specific conductance. This allows to determine all the antenna electrical specifications from the measured input impedance. In the following, the coupling properties of the ES antenna will be discussed in terms of the series resistance R_s. Strictly speaking, a more relevant parameter is the global conductance G_g linked to the total transmitted power P and the maximum voltage V_{Am} on the antenna by the formula:

$$P = \frac{G_g}{2} V_{Am}^2.$$

Under the above assumptions and in our experimental conditions, G_g can be shown to be approximately proportional to R_s and we shall be satisfied here to describe the ES antenna coupling in terms of this last quantity.

Two basic features of R_s can be observed in fig. 2. First, the resistance strongly decreases with power as can be seen at the beginning of the pulse where the power rises quickly. Second, R_s is nearly independent of B_T (the value of f/f_{ci} at the antenna outboard location, $r = 47$ cm, varies from 2 at the beginning of the RF pulse to 2.24 at the end).

These features are further illustrated by a statistical analysis. Fig. 4 shows that the decrease of the series resistance takes place at low power. For $P_{RF} \gtrsim 50$ kW, this dependence saturates and R_s becomes nearly independent of P_{RF}. This figure also shows an incrase of the series resistance with edge density (for which we take the line-averaged density at $r = 40$ cm, $\bar{n}_{e40}$ signal, as

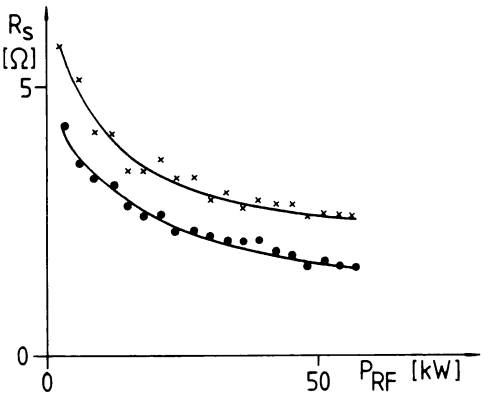

Fig. 4. Statistical analysis of the dependence of the series resistance on power. Data points are selected according to the value of $\bar{n}_{e40}$ at the time R_s is computed. ●: $\bar{n}_{e40} \in [0.8, 0.84]$, ×: $\bar{n}_{e40} \in [0.96, 1.]$. Statistics is over shots 35030–35090.

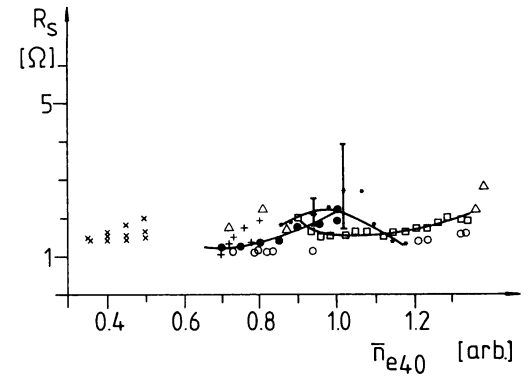

Fig. 5. Statistical analysis of the dependence of the series resistance on edge density ($\bar{n}_{e40}$). The different symbols correspond to different shot ranges and types: ●, shots 35030–35039, standard; *squares*, shots 35040–35047, outward horizontal plasma shift of 3 cm; *, shots 35049–35059, outward horizontal plasma shift of 3 cm, upward vertical plasma shift (a few cm), B_T scan; ×, shots 35602–35608, standard but $I_p = 220$ kA; +, shots 35732–35745, standard; Δ, shots 36061–36069, standard; ○, shots 36175–36192, FW-type ($B_T = 2$ T), outward horizontal plasma shift of 3 cm. Statistics have been made separately for each series of shots; the continuous lines represent the trends in specific series (●, *, *squares*). The error bars shown illustrate the fact that points falling outside the general stream have larger error bars than average.

representative). This tendency was seen several times in short series of shots. However, statistics over a larger series of shots, as in fig. 5, indicates that this dependence is, in fact, a weak one. The lines showing average trends for given shot series show that the opposite behaviour can be found in different sets. Similarly the path in the ($\bar{n}_{e40}$, R_s) plane for a single shot shows a

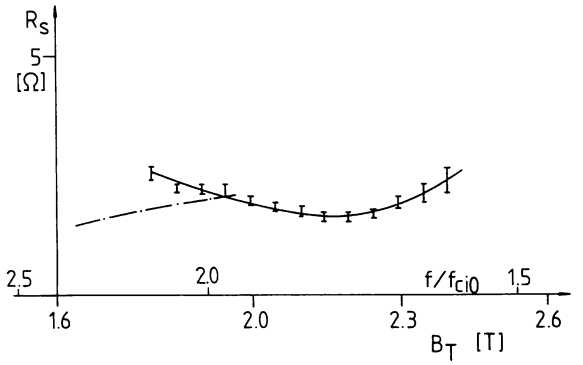

Fig. 6. Statistical dependence of R_s on B_T for a series of shots (35050–35056) with B_T scans. The solid line corresponds to $\bar{n}_{e40} \in [0.84, 0.96]$ and the dashed one to $\bar{n}_{e40} \in [1.05, 1.15]$.

large variety of behaviours (increases, decreases, independence), partly associated with the non-stationarity of the beginning of the pulse. If one compares, on fig. 5, the solid circles (plasma positionnned normally) and the squares (plasma shifted horizontally 3 cm outwards) one sees that the only effect of moving the plasma is to change the $\bar{n}_{e40}$ range. Fig. 6 shows a short statistics of coupling during B_T scans confirming the independence of R_s in a broader B_T range.

4.3. Comparison with theory

If the ES antenna is to be considered as an IBW launcher its behaviour is in complete contrast with the theoretical expectations. Indeed, according to theory, IBW coupling should show a sharp maximum when the cyclotron layer crosses the neighbourhood of the plasma edge and coupling should improve when the edge density is decreased [8–10]. However, in several IBW heating experiments with more conventional IBW launchers, the experimental resistance was found to display completely different behaviour from the theoretically expected one [11–13]. In the present case, even if the antenna is an IBW launcher, the situation is more complicated as the central conductor extends over some 40 cm in major radius. Thus it faces different values of the magnetic field, in contrast with the situation described by theoretical models. Therefore, one could expect some smoothing of the B_T dependence with respect to the theoretically idealized case.

A more fundamental question concerning the ES antenna is: what is the distribution of the launched power among FW and IBW? A coupling code has been developed [10] to answer these questions; unfortunately, up to now the plasma model is a uniform one, which is not ideal to compute the IBW/FW ratio. However, due to the approximate independence (or additivity) of FW and IBW coupling, some estimates can be obtained using this code and the FW one [14]. The first indications are that in general a large fraction of the power (80% or more) is launched on the FW branch unless coupling is optimized for IBW and the edge density is assumed very low (10^{18} m^{-3}). In poor IBW matching conditions (i.e. away from $f = 2f_{ci}$ at the edge) almost the totality of the power is launched on the FW branch. If this is confirmed by more accurate computations, the independence of coupling with respect to B_T can be understood and the n_e dependence might be more understandable. However then, the poor heating efficiencies obtained would have to be explained.

In view of the power dependence exhibited by the antenna resistance (fig. 4), further considerations can

enter the coupling discussion. As there was direct plasma flow to one central conductor, one can wonder whether part of the power was not dissipated through sheath effects, the system antenna-protection tiles playing the role of a double probe. Assuming an electron temperature of a few tens of eV, a density of some 10^{12} cm^{-3} at the central conductor's location and taking as probe area approximately twice the damaged area (16 cm^2) one gets Bohm ion saturation currents [15] compatible with the power thresholds for saturation observed experimentally ($\simeq$ 50 kW, fig.4). However the antenna voltage corresponding to this power threshold is $\simeq$ 1.7 kV, a value which is incompatible with double probe theory. If nevertheless the saturation can be associated with an anomalous loss mechanism, the parasitically dissipated power would be of the same order as the power coupled to the plasma bulk. The application of double probe theory made to the present RF situation is however very rough, and possibly irrelevant; clearly this point deserves more theoretical analysis.

4.4. Comparison with FW antenna

Using a typical value of R_s of 2 Ω the global conductance of the ES antenna is $G_g = 1.7 \times 10^{-3}\ \Omega^{-1}$. This is a factor of two less than the corresponding figure for the FW antenna in good loading conditions i.e. with a specific resistance $R = 5\ \Omega$/m [4].

5. Effects on the plasma edge

Fig. 2 gives a typical illustration of what happens during the ES antenna excitation: both the central line averaged density $\bar{n}_{e0}$ and the edge line averaged density $\bar{n}_{e40}$ increase, corresponding to a global density increase in the bulk of the plasma but weaker increases at the edge as shown on the contour plots of fig. 7. As soon as the RF is stopped, the density decreases, and vice-versa. At each RF switch on/off discontinuities appear in the contour lines; looking more closely at the location of these angular points they can be seen to be in phase with the RF at the edge but delayed by 25–35 ms in the central region $r \simeq 10$ cm. This indicates that a perturbation is propagated from the edge ($r \simeq 45$ cm) to the center.

On the other hand, all edge flux signals, shown on fig. 2c, *decrease* during the ES antenna operation. These fluxes are representative of the whole material area surrounding the plasma as they correspond to different positions in minor and major radius, poloidal angle and toroidal distance to the antenna. These decreases are

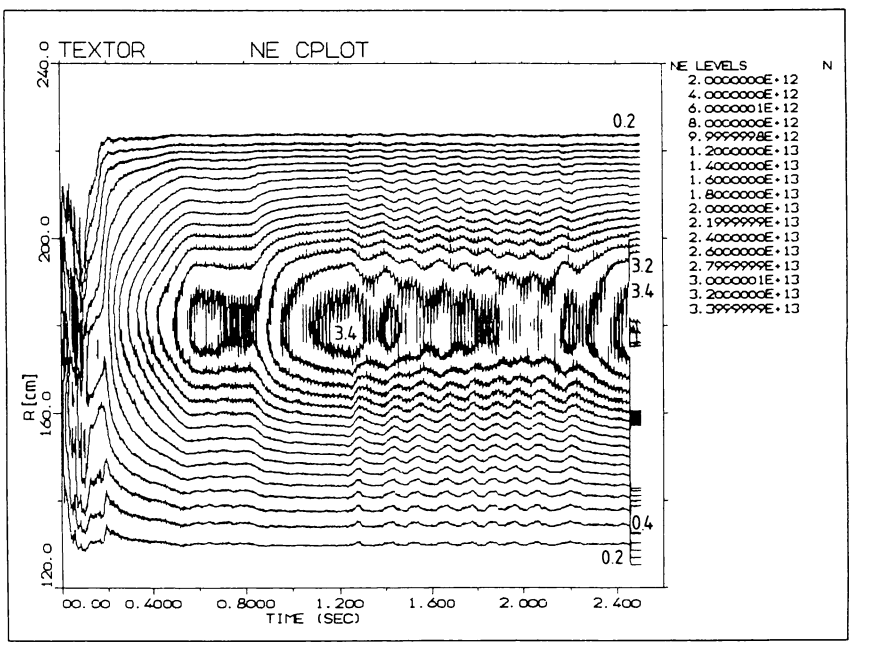

Fig. 7. Contour plot of the density considered as a function of time and major radius (shot 35054). The density jumps by 0.2×10^{19} m^{-3} between two successive curves. Curves are labelled in units of 10^{19} m^{-3}. Refer to fig. 2 for a comparison with the central density evolution and the RF pulse timing.

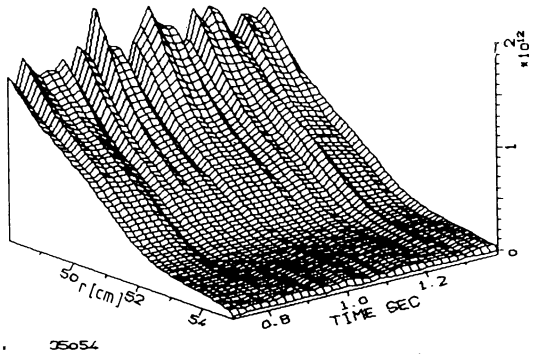

Fig. 8. Scrape-off density evolution as measured by lithium beam spectroscopy (A1Li). The ALT-II limiter is located at $r = 46$ cm and the antenna side limiters at $r = 47$ cm. Vertical scale in cm^{-3}.

relatively small and in many other shots, there is even no change at all. A slight decrease or invariance of the fluxes during the RF has been observed in all conditions (B_T, $\bar{n}_{e0}$, etc). The density being regulated, gas puffing normally stops at the density plateau; to maintain the density constant some slight puffing may follow; this is always stopped at the RF onset due to the associated density increase and there is no gas puff during RF.

For the shot of fig. 2, although the density increases everywhere in the plasma bulk, it slightly decreases in the scrape-off layer, as monitored by lithium beam measurements [5] shown in fig. 8. Again, the decrease is minor and even sometimes absent. Such a weak or nonexistent response of the scrape-off density profile has been observed with the two available lithium beam diagnostics, the one located close to the antenna and at the bottom, the other one toroidally opposite and measuring the outboard scrape-off density. Although not available for the shot of fig. 2, edge impurity lines (C I, O I) have also been monitored in front of the ALT-II toroidal belt limiter. Again, if there was a perturbation, it consisted of a small decrease.

The scrape-off electron temperature has only been measured a few times using scanning Langmuir probes [5]. The measured T_e were typical of the ohmic regime but no real ohmic/RF comparison could be made in the same shot due to insufficient data.

The central impurity line increases shown in fig. 2b are not dramatic in that, when normalized to density, they remain at the initial ohmic level during RF but fall below this level during the RF switch-off periods (which could possibly be explained by $\bar{n}_{e0}$ and T_e profile changes). For this shot, the radiation profiles remain hollow and the total radiated power increases from 100 kW in ohmic to 150 kW during RF. Therefore, one has to conclude that no significant contamination of the plasma has taken place.

The above described features are generally observed during ES pulses irrespective of plasma parameter or scenario choice. In particular, they were observed during FW type of shots in which both antenna types were operated. These results are very much in contrast to the significant perturbations created in the scrape-off by FW antennas [5].

As all edge fluxes and the scrape-off density remain unchanged or even decrease slightly while the bulk density significantly increases, it must be concluded that the particle confinement time increases during the ES antenna operation. From the existence of a finite perturbation propagation time observed in the density profiles, we can further guess that the particle diffusivity changes occur in the outer plasma region ($r <$ limiter radius) and are afterwards propagated towards the plasma center. It is to be noted that particle confinement time increase was observed in experiments using conventional IBW launchers [16,17].

6. Conclusions

According to theoretical investigations, the present ES launcher should mainly be a FW launcher. It is therefore maybe not suprising that, experimentally, it does not show the characteristics of an IBW coupler. However, its effects on both bulk and scrape-off plasma are also very different from the ones caused by the regular FW antennas. Part of these differences might be explained if a fraction of the power was lost in sheaths that screen the parallel electric field applied between the central conductor and the protecting limiter of the damaged antenna. The origin of the low voltage standoff cannot conclusively be assigned to electrostatic coupling due to the existence of direct plasma flow at localized spots towards this central conductor. This (unoptimized) ES launcher has only half the power coupling potential of the regular FW one. In most shots the choice of parameters was unfavourable to FW heating, however neither B_T scans nor operation in the FW-type shots showed indications of heating properties similar to those of the FW antennas. Also, there was no sign of magnetosonic global modes, as could have been

expected in low damping FW launch situations. Edge effects are in complete contrast to the ones induced by FW antennas and one has to conclude that the present ES coupling leads to improved particle confinement. It is to be noted that the fields imposed by the ES antenna (in particular a large radial electric field) are very different from those of a FW antenna and that screen fringing fields are absent. Further analytical studies of the present experimental observations could lead to a better understanding of the importance of field polarizations and of the role of the screen in the coupling and edge pertubation processes.

References

[1] F. Durodie et al., New ICRH system for TEXTOR compatible with ALT-II, Proc. 14th Symp. on Fusion Technology (SOFT), Avignon, 1 (1986) 729–735.

[2] J.M. Beuken et al., Comparison of ICRH heating scenarii and antenna configuration in TEXTOR, Proc. 15th European Conf. on Controlled Fusion and Plasma Heating, Dubrovnik, Europhysics Conf. Abstracts 12B, 2 (1988) 774–777.

[3] R.R. Weynants et al., Heating and confinement studies with low field side ICRH in TEXTOR, 12th Int. Conf. on Plasma Physics and Controlled Nuclear Fusion Research, Nice (IAEA, Vienna, 1988) IAEA-CN-50/E-2-1.

[4] A.M. Messiaen et al., Effect of antenna phasing and wall conditioning on ICRH in TEXTOR, Plasma Phys. Contr. Fus. 31 (1989) 921–939.

[5] G. Van Oost et al., ICRF/edge physics research on TEXTOR, invited paper, Fusion Engrg. Des. 12 (1990) 149–170, in these Proceedings.

[6] F. Durodie et al., Intallation, testing and first results of TEXTOR's new ICRH system, Proc. 15th Symp. Fusion Technology (SOFT), Utrecht, 1 (1988) 464–468.

[7] R. Van Nieuwenhove, F. Durodie, R. Koch and G. Van Oost, Capacitive probe measurements during RF heating on TEXTOR, Fusion Engrg. Des. 12 (1990) 203–207, in these Proceedings.

[8] W.N.-C. Sy, T. Amano, R. Ando, A. Fukuyama and T. Watari, Slow wave antenna coupling to ion Bernstein waves for plasma heating in ICRF, Nucl. Fus. 25 (1985) 795–803.

[9] M. Brambilla, Theory of Bernstein wave coupling with loop antennas, Nucl. Fus. 28 (1988) 549–563.

[10] R. Koch, V. Nys, D. Van Eester and F. Durodie, Full hot plasma ray tracing, waveguide coupling and application to ion Bernstein wave heating, LPP ERM/KMS Brussels Report No. 89 (1989).

[11] Y. Takase, J.D. Moody, C.L. Fiore, F.S. McDermott, M. Porkolab and J. Squire, Study of directly launched ion Bernstein waves in a tokamak, Phys. Rev. Lett. 59 (1987) 1201–1204.

[12] S. Shinohara, O. Naito and K. Miyamoto, Dependence of resistive loading on antenna orientation for ICRF waves in a tokomak, Nucl. Fus. 26 (1986) 1097–1102.

[13] R.I. Pinsker, M.J. Mayberry, M. Prokolab and R. Prater, High power ion Bernstein wave experiments on DIII-D, Proc. 8th Topical Conf. on RF Power in Plasmas, Irvine (1989) pp. 314–317.

[14] R. Koch et al., ICRF theoretical studies and interpretation of modulation experiments on JET, LPP ERM/KMS Brussels Report No. 87 (1988).

[15] F.F. Chen, Electric probes, in: Plasma Diagnostic Techniques, eds., R.H. Huddlestone and L. Leonard (Academic Press, New York, 1965) pp. 138–151.

[16] M. Ono et al., Ion Bernstein wave heating experiments on PLT, 11th Int. Conf. on Plasma Physics and Controlled Nuclear Fusion Research, Kyoto, Nucl. Fus. Suppl. 1 (1987) 477–484.

[17] M. Porkolab et al., Radiofrequency heating and current drive experiments on Alcator C and Versator II, 11th Int. Conf. on Plasma Physics and Controlled Nuclear Fusion Research, Kyoto, Nucl. Fus. Suppl. 1 (1987) 509–523.